

Putting the Segment Anything Model to the Test with 3D Knee MRI - A Comparison with State-of-the-Art Performance

Oliver Mills¹

scojm@leeds.ac.uk

Nishant Ravikumar¹

N.Ravikumar@leeds.ac.uk

Philip Conaghan^{1, 2}

P.Conaghan@leeds.ac.uk

Samuel D. Relton¹

S.D.Relton@leeds.ac.uk

¹ University of Leeds

Leeds, UK

² NIHR Leeds Biomedical Research

Centre

Leeds, UK

Abstract

Menisci are cartilaginous tissue found within the knee that contribute to joint lubrication and weight dispersal. Damage to menisci can lead to onset and progression of knee osteoarthritis (OA), a condition that is a leading cause of disability, and for which there are few effective therapies. Accurate automated segmentation of menisci would allow for earlier detection and treatment of meniscal abnormalities, as well as shedding more light on the role the menisci play in OA pathogenesis. Focus in this area has mainly used variants of convolutional networks, but there has been no attempt to utilise recent large vision transformer segmentation models. The Segment Anything Model (SAM) is a so-called foundation segmentation model, which has been found useful across a range of different tasks due to the large volume of data used for training the model. In this study, SAM was adapted to perform fully-automated segmentation of menisci from 3D knee magnetic resonance images. A 3D U-Net was also trained as a baseline. It was found that, when fine-tuning only the decoder, SAM was unable to compete with 3D U-Net, achieving a Dice score of 0.81 ± 0.03 , compared to 0.87 ± 0.03 , on a held-out test set. When fine-tuning SAM end-to-end, a Dice score of 0.87 ± 0.03 was achieved. The performance of both the end-to-end trained SAM configuration and the 3D U-Net were comparable to the winning Dice score (0.88 ± 0.03) in the IWOAI Knee MRI Segmentation Challenge 2019. Performance in terms of the Hausdorff Distance showed that both configurations of SAM were inferior to 3D U-Net in matching the meniscus morphology. Results demonstrated that, despite its generalisability, SAM was unable to outperform a basic 3D U-Net in meniscus segmentation, and may not be suitable for similar 3D medical image segmentation tasks also involving fine anatomical structures with low contrast and poorly-defined boundaries.

1 Introduction

Osteoarthritis (OA) is one of the leading causes of disability worldwide, and costs the NHS over £3 billion annually [1]. It is a condition where joint cartilage degeneration causes pain and stiffness [1]. Knee OA is a particularly common type of OA, and with an aging population and rising obesity levels [2], over 8 million people are forecast to have symptomatic knee OA in the UK by 2035 [36]. Knee OA is a heterogeneous disease [26], and the roles of different tissues in the onset of the disease are not well understood in literature. The tissues of focus in this study were the menisci, two semi-lunar, wedge-shaped structures found within the knee joint [25], which play an important role in load-bearing, as well as the shock distribution and lubrication of the joint [12, 25]. Multiple studies have shown that meniscal degeneration and tears are highly correlated with the presence of knee osteoarthritis [4, 11, 19], but the role the meniscus plays in the disease pathway is still unclear. A better understanding of the role of the menisci in this regard has the potential to improve early treatment and reduce the burden on health services.

Current methods for assessing meniscal degeneration include ‘eyeballing’ magnetic resonance (MR) scans and arthroscopy. These methods are often ambiguous at assessing the level of meniscal degeneration [32]. Image segmentation of MR scans provides a way to better visualise and analyse the geometric properties of the meniscus [21]. However, manual segmentation is time-consuming and often has poor inter- and intra-individual reliability [28]. Segmentation of the menisci in MR scans is particularly challenging, as the contrast of the menisci overlaps with other nearby tissues such as femoral and tibial cartilage [32]. Automated segmentation could provide a quicker, objective and more accurate way of segmenting the meniscus [22], and in turn shed more light on the role it plays in OA development.

1.1 Deep Learning in Medical Image Analysis

Since the introduction of convolutional neural networks (CNNs) in 2012 through AlexNet [20], which outperformed all other models when classifying the ImageNet data set, CNNs have been the most popular deep learning method for image analysis tasks. CNNs utilise kernels, which are convolution matrices that allow both small and large scale spatial features to be extracted from input images. In the past decade, CNNs have shown great success when applied to a range of medical image analysis tasks [7, 23, 29, 34, 40]. Many applications of CNNs to medical image analysis are now competing with, and even surpassing manual assessment by clinical experts[41].

In the field of image segmentation, U-Net [33] is one of most popular CNN-based methods. The network is made up of two parts: an encoder, where successive convolutional and pooling layers are used to learn a hierarchy of features across spatial scales and reduce the image to a low-dimensional feature representation; and a decoder, where the feature representation is then upsampled to the original image size, often output in the form of a segmentation mask. U-Net also utilises skip-connections, where different stages on the down-sampling path (in the encoder) are concatenated with the corresponding stage on the up-sampling paths (in the decoder) [33]. This is done to provide contextual features at the same spatial scale learned in the encoder and reduce information loss during training. U-Net has shown great performance on a range of medical segmentation tasks [35]. A 3D version of U-Net was proposed to allow volumetric segmentation without the need for going slice-wise through a 3D image [8]. Currently, variations of the U-Net design are consistently among the top-performing models in both 2D and 3D medical image segmentation challenges [10, 13].

Recently, image segmentation has been attempted with vision transformer (ViT)-based model architectures, which use attention modules to generate feature embeddings of images. Perhaps the most widely-known example of a ViT segmentation model is the Segment Anything Model (SAM) [18]. SAM was introduced as a foundation 2D image segmentation model, with the ability to generalise to tasks outside the domain of its vast training set, SA-1B, which was made up of over 1.1 million images and 1 billion masks. SAM is also promptable, where point, box, or mask prompts can be provided to help the model generate segmentation masks.

Since the development of SAM, attention has turned to applying it to medical images. It has been demonstrated that, without any fine-tuning, SAM has the capacity to compete with state-of-the-art segmentation models on certain medical image tasks, albeit only with excessive prompting [8]. However, other studies have found that SAM struggles in tasks where boundaries are not clearly defined [38], one example being when attempting skin lesion segmentation [16]. This is particularly relevant to segmentation of the meniscus, where boundaries are unclear due to the overlap of contrast with neighbouring tissue.

Other studies have tried to fine-tune SAM for medical segmentation tasks [6, 40, 42]. The first attempt to adapt SAM for medical images fine-tuned the mask decoder on a range of medical images of different modalities, and saw an increase in performance [24]. However, this study provided prompts during training, so the model was not fully automated. Even after fine-tuning, it was found that SAM struggled with segmentation involving regions that were small, low-contrast, and with unclear boundaries, all of which apply to the meniscus.

In this study, the aim was to investigate whether SAM could be fine-tuned and adapted to perform automatic segmentation of menisci from 3D knee MR images without providing prompts, which has not yet been attempted. A 3D U-Net was trained using randomly initialised weights on the same data set, to compare SAM to current state-of-the-art performance. The performance of the trained segmentation models was then qualitatively and quantitatively assessed in terms of the similarity between the predicted segmentation masks and the manually generated ground truth masks.

2 Materials and Methods

2.1 Data

The data used in this study was the same used in the International Workshop on Osteoarthritis Imaging Knee MRI Segmentation Challenge 2019 (IWOAI 2019) [9]. The data used was a subset of the Osteoarthritis Initiative (OAI). The OAI contains 3D knee Double-Echo-Steady-State (DESS) MRI of 4796 patients (comprising men and women, aged 45-79) at multiple time-points, who were at risk of femoral-tibial knee osteoarthritis [40, 41], making it a valuable resource for studying longitudinal changes of the knee joint. The subset used in this study contained 88 patients at two time points (baseline and 1-year follow-up), each having corresponding manual segmentations of medial and lateral menisci, which were generated by a single expert segmenter from Stryker Imorphics [9]. Each image was 384 by 384, with 160 slices in the sagittal direction. The images had a resolution of $(0.365\text{mm} \times 0.456\text{mm} \times 0.7\text{mm}$ slice thickness) [41].

The 88 patients were split into train, validation and test groups of 60, 14 and 14 respectively, resulting in 176 images split into sets of 120 train, 28 validation, and 28 test images. Splits were done in consistency with the IWOAI 2019 challenge, where Kellgren-Lawrence score, BMI, and sex were approximately equally distributed across the splits [9].

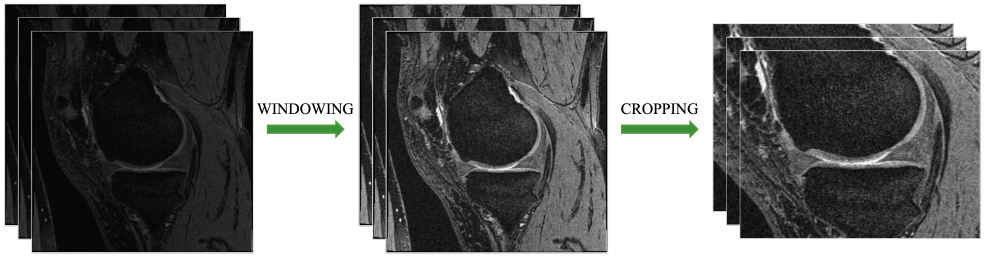


Figure 1: Preprocessing steps performed on the MR Images before model training. Windowing was performed between 0 and 0.005. The cropped region was selected based on the variation in location of ground truths in the train and validation sets.

2.2 Preprocessing

Before training, windowing was performed on the MRI images, clipping the values to be between 0 and 0.005, which were then re-scaled between 0 and 1. This clipping window was selected after viewing the intensity distribution in the images. Clipping the intensity range allowed for greater relative contrast between different artifacts in the joint after re-scaling (Fig. 1). The images were then cropped from $384 \times 384 \times 160$ down to $200 \times 256 \times 160$. The cropped region was selected so that all train/validation meniscus masks fell within it, with an extra margin of safety (~ 20 voxels) given in all directions. Cropping resulted in the menisci taking up a larger volume of the image, as well as reducing the computational memory requirements of model training. The test images were cropped in the same way.

2.3 3D U-Net

The 3D U-Net architecture used took inspiration largely from the original paper that proposed U-Net [53], with 3D convolution operations instead of 2D. The model used 16 feature maps in the first convolution block, with this number doubling in each successive block until the bottleneck. The encoder and decoder were each made up of 3 convolution blocks.

2.4 Segment Anything Model

The base ViT version of SAM was used in this project due to the sizeable increase in computational demands from using the ViT Large and ViT Huge versions, which have been reported to provide only marginal improvements in performance in previous studies [18, 24]. To fine-tune SAM, each 3D image was split into 160 separate 2D slices along the sagittal direction, the same being done with the 3D manual segmentations to generate corresponding 2D ground truths. The train, validation and test data splits were kept consistent, so each split now contained the number of 3D images previously mentioned, multiplied by 160. This resulted in train, validation and test splits of size 19200, 4480 and 4480 respectively. Each slice was upsampled using bilinear interpolation and padded. Three copies of this upsampled image were concatenated, resulting in a $1024 \times 1024 \times 3$ image in the accepted input format for SAM. When evaluating, all 2D slice predictions were stacked to form a 3D mask, which was compared to the ground truth to evaluate performance. SAM was adapted to not take in prompts and output only a single mask, ensuring that the segmentation was fully automated.

2.5 Evaluation Metrics

2.5.1 Dice Score

The Dice score is a standard metric for evaluating segmentation performance. Given a ground truth mask, GT , and a segmentation prediction, SP , the Dice score is given by

$$Dice = \frac{2 \times |GT \cap SP|}{|GT| + |SP|}. \quad (1)$$

2.5.2 Hausdorff Distance

The Dice score measures the overlap of two masks, but gives no information on how wrong any false positives are. Two masks could have a high overlap but poor matching on specific structures of interest. To shed light on this, it is useful to include a spatial distance based metric. The Hausdorff Distance is one example of a distance metric. For each point on the surface of the prediction mask SP , the distance to the closest point on the surface of GT is measured, and vice versa. The Hausdorff Distance is the maximum of these values, providing information on the worst-matching region of SP to GT . However, the maximum Hausdorff Distance can be misleading in the presence of noise and any ground truth outliers [87], so the 95% percentile Hausdorff Distance was used [14].

2.5.3 Average Transverse Thickness

It has been suggested that the meniscal thickness is a biomarker for Osteoarthritis [11, 89]. Therefore, the average transverse thickness of the ground truth and predicted masks were calculated and compared to see how well the predicted masks preserved the thickness of the menisci. This was done by averaging the total volume over the number of non-zero columns in the transverse plane.

2.6 Model Training

SAM was fine-tuned in two different configurations. In the first, the image encoder was frozen and only the mask decoder was trained (SAM 1). This greatly reduced the computational requirements for re-training the model, by lowering the number of trainable parameters in the model from over 91 million down to 4 million. In the second configuration, the model was trained end-to-end with all parameters unfrozen (SAM 2).

The 3D U-Net was trained using a loss function comprising of an unweighted combination of binary cross-entropy (BCE) loss and dice loss, which is simply $1 - Dice$. Model convergence was found to be quicker and smoother using this loss function compared to

Table 1: Summary of parameters used for training the different models. SAM was fine-tuned in two ways: by training the mask decoder (SAM 1), and by training end-to-end (SAM 2).

| <i>Model</i> | <i>No. of trainable params</i> | <i>Batch Size</i> | <i>Learning Rate</i> | <i>Loss</i> |
|--------------|--------------------------------|-------------------|----------------------|-------------|
| SAM 1 | 4,058,340 | 8 | $5e - 6$ | BCE |
| SAM 2 | 93,735,472 | 16 | $5e - 7$ | BCE |
| 3D U-Net | 2,041,825 | 4 | $1e - 3$ | BCE + Dice |

Table 2: A comparison of model performance metrics on the test set. Average Thickness Difference was calculated by taking the mean of the predicted mask thickness subtracted from the ground truth thickness for each test case. SAM was fine-tuned both by training only the mask decoder (SAM 1), and by training end-to-end (SAM 2). Hausdorff Distance and Average Thickness Difference are reported in millimeters (mm).

| <i>Model</i> | <i>Dice score</i> | <i>Hausdorff Distance</i> | <i>Average Thickness Difference</i> |
|--------------|-----------------------------------|---------------------------------|-------------------------------------|
| SAM 1 | 0.81 ± 0.03 | 3.1 ± 1.9 | -0.17 ± 0.2 |
| SAM 2 | 0.87 ± 0.03 | 2.4 ± 1.4 | 0.07 ± 0.12 |
| 3D U-Net | 0.87 ± 0.03 | 1.8 ± 0.8 | 0.03 ± 0.15 |

purely BCE or dice loss [15]. SAM was trained using BCE loss, due to some slices in the training set containing no ground truth. In this case, dice loss would become large, due to no overlap, and would lead to unstable training. The Adam optimiser was used for training both the 3D U-Net and SAM. Random grid searches were performed to select the optimal batch size and learning rate (as well as number of kernels for 3D U-Net) for each of the models (Table 1). Training was stopped once the validation loss failed to decrease for 5 epochs.

3 Results and Discussion

SAM 1 achieved the worst score on all metrics (Table 2), suggesting that, despite SAM’s large pre-trained encoder, the extracted features were not good enough to produce competitive meniscus segmentations. Training SAM end-to-end improved Dice score performance, matching 3D U-Net. In the IWOAI 2019 challenge, the highest-performing entry achieved a Dice score of 0.88 ± 0.3 on the test set [16], meaning that SAM 2 was able to compete with state-of-the-art performance despite lacking 3D context. This also demonstrated the impressive segmentation ability of the vanilla 3D U-Net, achieving a similarly high score.

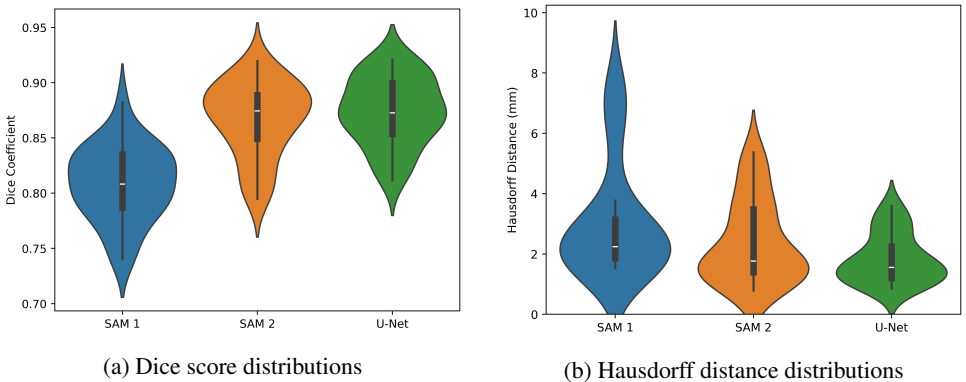


Figure 2: Violin plots showing the distributions of the dice score (a) and Hausdorff distance (b) of the three model configurations when predicting on the test set. In the violin interior, a box plot is shown. In SAM 1, only the mask decoder was trained. In SAM 2, the model was trained end-to-end.

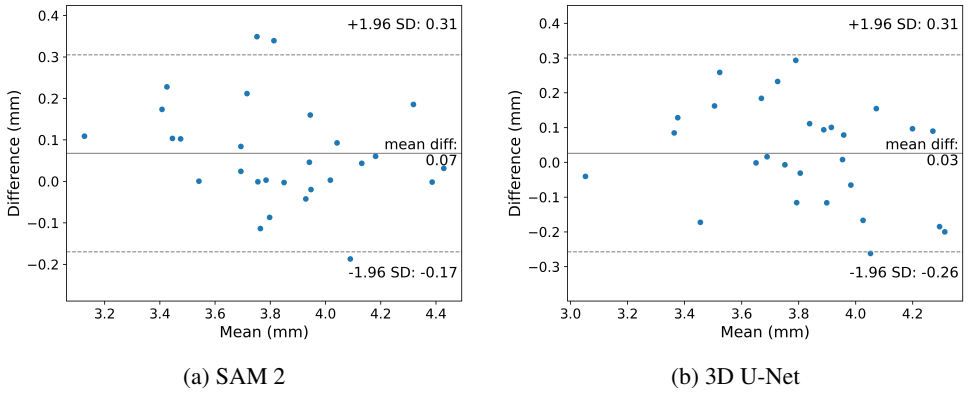


Figure 3: Bland-Altman plots showing the difference in transverse thickness between masks generated by SAM 2 (a) and 3D U-Net (b). The difference was calculated by subtracting the ground truth thickness from the generated mask thickness.

There was little to separate SAM 2 and 3D U-Net on mean values alone, so the distributions of the Dice score and Hausdorff Distance across the test set were plotted (Fig. 2). When looking at Dice Score, SAM 2 and U-Net had a similar mean and interquartile range, but SAM 2 performed more poorly on a small number of cases (2a). Fig. 2b indicates that despite the improvement from training SAM end-to-end compared to training only the decoder, 3D U-Net has both a lower mean and less variability than both SAM configurations in terms of the Hausdorff distance. This suggests that 3D U-Net is superior at predicting masks that closely match the geometry of the menisci consistently, without introducing errant spatial artifacts.

SAM 2 and U-Net both outperformed SAM 1 in preserving the thickness of the menisci. Bland-Altman plots in Fig. 3 summarise the agreement between the predicted average thickness of the predicted meniscal masks with that of the ground truths. In Bland-Altman plots, the difference between two values is plotted against the mean of the two values [27]. Looking at Fig. 3, it is seen that there is little correlation between the size of the menisci and any under- or over-prediction in thickness. Both SAM 2 and 3D U-Net had a positive average thickness difference, implying that the models overestimated the meniscal thickness, with U-Net overestimating to a lesser degree. These differences were sub-voxel in both cases, so thickness was well-preserved.

3.1 Case Analyses

Two selected cases from the test set, and the corresponding model predictions, are shown in Fig. 4. One abnormal case in the test set contained a medial meniscus that was fully separated in the middle (a). The models were only exposed to a single case in the train set with a similar morphology. Predicted masks for this test case are shown in (b-d). It can be seen that, despite only being exposed to one similar case in training, 3D U-Net correctly reproduces the two fully-detached medial meniscus segments. Both SAM configurations struggle to replicate this feature. Another example was selected due to what appears to be a partial meniscectomy on the posterior horn of the medial meniscus (white arrow in 4e). The predicted masks for this case indicate that SAM 1 fails to recognise this feature, while

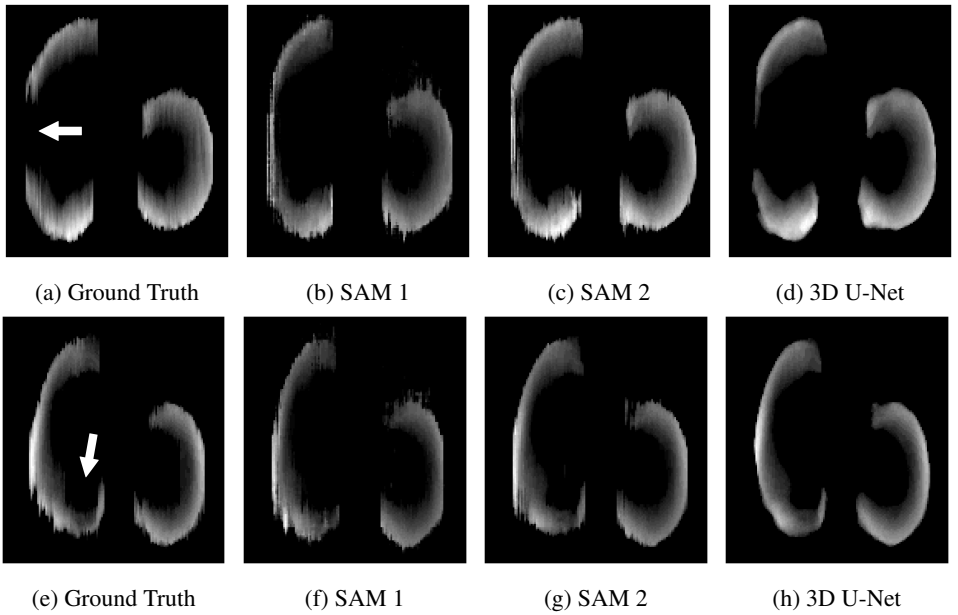


Figure 4: Two atypical examples from the test dataset that visually compare the masks predicted by the segmentation models investigated with the ground truth. In (a), a ground truth mask is shown where the medial meniscus was separated into two (white arrow). (b-d) are the generated masks from SAM 1, SAM 2, and 3D U-Net respectively. (e) shows a test case with what appears to be a partial meniscectomy on the posterior medial meniscal horn (white arrow). (f-h) are again the generated masks from SAM 1, SAM 2, and 3D U-Net respectively. All images in this figure were created by summing the 3D masks through the inferior-superior axis of the body, as if looking down on the mask from above. The brighter a pixel, the thicker the meniscus in this transverse position.

SAM 2 and 3D U-Net both do. This demonstrates that training SAM end-to-end improved the ability of the model to extract anomalous morphological features of menisci.

Fig. 5 displays surface mesh representations of masks generated from a test set image by SAM 2 and U-Net, along with the corresponding ground truth. The 3D meshes were produced using ITK-SNAP. Both SAM 2 and U-Net scored the lowest Dice coefficient on this image, so the meshes are a good example of where SAM 2 and U-Net fail to accurately perform meniscus segmentation. The first feature to highlight is that SAM 2 fails to replicate the narrowing near the middle of the medial meniscus. U-Net does much better at reproducing the general geometry of the ground truth. SAM 2 also struggles to keep the menisci as a contained volume, with flecks of unattached positive predictions seen in Fig. 5b. U-Net did not suffer from this problem, which likely stemmed from SAM 2 lacking 3D contextual information unlike the former.

SAM configurations often outputted masks containing small isolated islands of positive prediction (e.g. Fig. 5b), struggling to output consistent intact volumes. Through performing connected component analysis on the ground truths and generated masks, it was seen that predictions from SAM 1 and 2 contained an average of 46.9 and 10.2 components respectively, compared to the ground truths which contained an average of 2.1. In contrast, masks



Figure 5: Surface mesh representations of the worst-performing (Dice score) predicted masks of 3D U-Net and end-to-end trained SAM (SAM 2) from the test knee MRI set, shown alongside the corresponding ground truth. The meshes contain both the lateral and medial menisci, which are seen on the left and right of each subfigure.

generated by 3D U-Net contained very few regions disconnected from the main segmentation bodies (average number of connected components of 2.3). This is desirable, because less post-processing would be required if the generated masks were to be analysed geometrically.

Figures 4 and 5 show that the masks generated by 3D U-Net are smoother, whereas the texture of the SAM masks more closely matches the ground truth. This could be due to the ground truths being annotated slice-wise leading to staircase artifacts that are not faithful 3D representations of the menisci. In this case, the Dice score may be punishing the 3D U-Net model for generating smoother masks than the ground truths, which may actually more closely resemble the true 3D structure of the menisci. There was concern that this smoothing effect might result in 3D U-Net smoothing out smaller features, but the Hausdorff distance results show that the smoothing is not compromising the model’s ability to match the meniscus geometry.

One problem with the data set used in this study was that, apart from two cases in the training data and one in the test data, all menisci were fully intact. When menisci are highly degenerate, they may no longer be two semi-lunar structures. Segmenting menisci once they have broken down into multiple pieces would be a far more challenging task, but there was little scope here to monitor performance on such cases. Another issue was that the ground truths were annotated by a single expert, so prone to more bias and error than if multiple segmenters had resolved conflicts between themselves.

4 Conclusion

Despite its generalisability, SAM, when only fine-tuning the decoder, performed significantly worse than a 3D U-Net when segmenting the menisci from MR images (Dice score 0.81 ± 0.03 compared to 0.87 ± 0.03). When training SAM end-to-end, comparable results were obtained (Dice score 0.87 ± 0.03). This demonstrates that fine-tuning the SAM encoder, to better extract task-relevant features, can compete with state-of-the-art performance (0.88 ± 0.03). However, the Hausdorff Distance showed that SAM was inferior to 3D U-Net in preserving the spatial features of the menisci, showing that it may not be suitable for deriving meaningful biomarkers from the menisci for monitoring the progression of OA. These weaknesses of SAM may also be relevant for other medical image segmentation tasks involving fine anatomical structures with low contrast and unclear boundaries.

5 Future Work

In the data set used, each patient had two MR scans at different points in time. For patients with noticeable changes between the two scans, it would be beneficial to analyse the ability of models to identify these changes. For example, if the thickness has changed over time, this should be mirrored in the generated masks.

Once a suitable model has been selected, automated segmentation of menisci could be performed for the entire OAI cohort. Geometric analysis of the generated masks, in combination with patients' clinical data, has the potential to reveal important OA biomarkers, both for onset and progression.

Acknowledgments

We would like to thank the OAI and its participants for creating this publicly available data set, and Dr Akshay Chaudhari (Stanford University) for providing the subset of the OAI used for the IWOAI 2019 challenge. This work made use of time on both ARC4, part of the High Performance Computing facilities at the University of Leeds, and Tier 2 HPC facility JADE2 (funded by EPSRC, EP/T022205/1). This work was funded by EPSRC (EP/S024336/1). Code is available at: https://github.com/oliverjml/BMVC_menisc_seg.

References

- [1] Reza Azad, Ehsan Khodapanah Aghdam, Amelie Rauland, Yiwei Jia, Atlas Hadadi Avval, Afshin Bozorgpour, Sanaz Karimijafarbigloo, Joseph Paul Cohen, Ehsan Adeli, and Dorit Merhof. Medical Image Segmentation Review: The success of U-Net, November 2022. URL <http://arxiv.org/abs/2211.14830>. arXiv:2211.14830 [cs, eess].
- [2] Timothy Bhattacharyya, Daniel Gale, Peter Dewire, Saara Totterman, M. Elon Gale, Sara McLaughlin, Thomas A. Einhorn, and David T. Felson. The Clinical Importance of Meniscal Tears Demonstrated by Magnetic Resonance Imaging in Osteoarthritis of the Knee*. *JBJS*, 85(1):4, January 2003. ISSN 0021-9355. URL https://journals.lww.com/jbjsjournal/Fulltext/2003/01000/The_Clinical_Importance_of_Meniscal_Tears.2.aspx.
- [3] Joseph A. Buckwalter, Charles Saltzman, and Thomas Brown. The Impact of Osteoarthritis: Implications for Research. *Clinical Orthopaedics and Related Research (1976-2007)*, 427:S6, October 2004. doi: 10.1097/01.blo.0000143938.30681.9d. URL https://journals.lww.com/corr/abstract/2004/10001/the_impact_of_osteoarthritis__implications_for.4.aspx.
- [4] A. Chen, C. Gupte, K. Akhtar, P. Smith, and J. Cobb. The Global Economic Cost of Osteoarthritis: How the UK Compares. *Arthritis*, 2012:698709, 2012. ISSN 2090-1984. doi: 10.1155/2012/698709. URL <https://www.ncbi.nlm.nih.gov/pmc/articles/PMC3467755/>.
- [5] Junlong Cheng, Jin Ye, Zhongying Deng, Jianpin Chen, Tianbin Li, Haoyu Wang, Yanzhou Su, Ziyang Huang, Jilong Chen, Lei Jiang, Hui Sun, Junjun He, Shaot-

- ing Zhang, Min Zhu, and Yu Qiao. SAM-Med2D, August 2023. URL <http://arxiv.org/abs/2308.16184>. arXiv:2308.16184 [cs].
- [6] Ozgun Cicek, Ahmed Abdulkadir, Soeren S. Lienkamp, Thomas Brox, and Olaf Ronneberger. 3D U-Net: Learning Dense Volumetric Segmentation from Sparse Annotation. In Sebastien Ourselin, Leo Joskowicz, Mert R. Sabuncu, Gozde Unal, and William Wells, editors, *Medical Image Computing and Computer-Assisted Intervention – MICCAI 2016*, Lecture Notes in Computer Science, pages 424–432, Cham, 2016. Springer International Publishing. ISBN 978-3-319-46723-8. doi: 10.1007/978-3-319-46723-8_49.
- [7] Francesco Ciompi, Bartjan de Hoop, Sarah J. van Riel, Kaman Chung, Ernst Th. Scholten, Matthijs Oudkerk, Pim A. de Jong, Mathias Prokop, and Bram van Ginneken. Automatic classification of pulmonary peri-fissural nodules in computed tomography using an ensemble of 2D views and a convolutional neural network out-of-the-box. *Medical Image Analysis*, 26(1):195–202, December 2015. ISSN 1361-8415. doi: 10.1016/j.media.2015.08.001. URL <https://www.sciencedirect.com/science/article/pii/S1361841515001255>.
- [8] Ruining Deng, Can Cui, Quan Liu, Tianyuan Yao, Lucas W. Remedios, Shunxing Bao, Bennett A. Landman, Lee E. Wheless, Lori A. Coburn, Keith T. Wilson, Yaohong Wang, Shilin Zhao, Agnes B. Fogo, Haichun Yang, Yucheng Tang, and Yuankai Huo. Segment Anything Model (SAM) for Digital Pathology: Assess Zero-shot Segmentation on Whole Slide Imaging, April 2023. URL <http://arxiv.org/abs/2304.04155>. arXiv:2304.04155 [cs, eess].
- [9] Arjun D. Desai, Francesco Caliva, Claudia Iriondo, Naji Khosravan, Aliasghar Mortazi, Sachin Jambawalikar, Drew Torigian, Jutta Ellermann, Mehmet Akcakaya, Ulas Bagci, Radhika Tibrewala, Io Flament, Matthew O’Brien, Sharmila Majumdar, Mathias Perslev, Akshay Pai, Christian Igel, Erik B. Dam, Sibaji Gaj, Mingrui Yang, Kunio Nakamura, Xiaojuan Li, Cem M. Deniz, Vladimir Juras, Ravinder Regatte, Garry E. Gold, Brian A. Hargreaves, Valentina Pedoia, and Akshay S. Chaudhari. The International Workshop on Osteoarthritis Imaging Knee MRI Segmentation Challenge: A Multi-Institute Evaluation and Analysis Framework on a Standardized Dataset, May 2020. URL <http://arxiv.org/abs/2004.14003>. arXiv:2004.14003 [cs, eess].
- [10] B. Dube, M. A. Bowes, S. R. Kingsbury, E. M. A. Hensor, S. Muzumdar, and P. G. Conaghan. Where does meniscal damage progress most rapidly? An analysis using three-dimensional shape models on data from the Osteoarthritis Initiative. *Osteoarthritis and Cartilage*, 26(1):62–71, January 2018. ISSN 1063-4584. doi: 10.1016/j.joca.2017.10.012. URL <https://www.sciencedirect.com/science/article/pii/S1063458417312657>.
- [11] M. Englund, J. Niu, A. Guermazi, F. W. Roemer, D. J. Hunter, J. A. Lynch, C. E. Lewis, J. Torner, M. C. Nevitt, Y. Q. Zhang, and D. T. Felson. Effect of meniscal damage on the development of frequent knee pain, aching, or stiffness. *Arthritis and Rheumatism*, 56(12):4048–4054, December 2007. ISSN 0004-3591. doi: 10.1002/art.23071.
- [12] Donald C. Fithian, Michael A. Kelly, and Van C. Mow. Material Properties and Structure-Function Relationships in the Menisci. *Clinical Orthopaedics*

- and Related Research*®, 252:19, March 1990. ISSN 0009-921X. URL https://journals.lww.com/clinorthop/Abstract/1990/03000/Material_Properties_and_Structure_Function.4.aspx.
- [13] Nicholas Heller, Fabian Isensee, Klaus H. Maier-Hein, Xiaoshuai Hou, Chunmei Xie, Fengyi Li, Yang Nan, Guangrui Mu, Zhiyong Lin, Miofei Han, Guang Yao, Yaozong Gao, Yao Zhang, Yixin Wang, Feng Hou, Jiawei Yang, Guangwei Xiong, Jiang Tian, Cheng Zhong, Jun Ma, Jack Rickman, Joshua Dean, Bethany Stai, Resha Tejpal, Makinna Oestreich, Paul Blake, Heather Kaluzniak, Shaneabbas Raza, Joel Rosenberg, Keenan Moore, Edward Walczak, Zachary Rengel, Zach Edgerton, Ranveer Vasdev, Matthew Peterson, Sean McSweeney, Sarah Peterson, Arveen Kalapara, Niranjan Sathianathan, Nikolaos Papanikolopoulos, and Christopher Weight. The state of the art in kidney and kidney tumor segmentation in contrast-enhanced CT imaging: Results of the KiTS19 challenge. *Medical Image Analysis*, 67:101821, January 2021. ISSN 1361-8415. doi: 10.1016/j.media.2020.101821. URL <https://www.sciencedirect.com/science/article/pii/S1361841520301857>.
 - [14] D.P. Huttenlocher, G.A. Klanderman, and W.J. Rucklidge. Comparing images using the Hausdorff distance. *IEEE Transactions on Pattern Analysis and Machine Intelligence*, 15(9):850–863, September 1993. ISSN 1939-3539. doi: 10.1109/34.232073. Conference Name: IEEE Transactions on Pattern Analysis and Machine Intelligence.
 - [15] Shruti Jadon. A survey of loss functions for semantic segmentation. In *2020 IEEE Conference on Computational Intelligence in Bioinformatics and Computational Biology (CIBCB)*, pages 1–7, October 2020. doi: 10.1109/CIBCB48159.2020.9277638. URL <http://arxiv.org/abs/2006.14822>. arXiv:2006.14822 [cs, eess].
 - [16] Wei Ji, Jingjing Li, Qi Bi, Tingwei Liu, Wenbo Li, and Li Cheng. Segment Anything Is Not Always Perfect: An Investigation of SAM on Different Real-world Applications, May 2023. URL <http://arxiv.org/abs/2304.05750>. arXiv:2304.05750 [cs].
 - [17] Victoria L. Johnson and David J. Hunter. The epidemiology of osteoarthritis. *Best Practice & Research Clinical Rheumatology*, 28(1):5–15, February 2014. ISSN 1521-6942. doi: 10.1016/j.berh.2014.01.004. URL <https://www.sciencedirect.com/science/article/pii/S1521694214000059>.
 - [18] Alexander Kirillov, Eric Mintun, Nikhila Ravi, Hanzi Mao, Chloe Rolland, Laura Gustafson, Tete Xiao, Spencer Whitehead, Alexander C. Berg, Wan-Yen Lo, Piotr Dollár, and Ross Girshick. Segment Anything, April 2023. URL <http://arxiv.org/abs/2304.02643>. arXiv:2304.02643 [cs].
 - [19] Peter R. Kornaat, Johan L. Bloem, Ruth Y. T. Ceulemans, Naghmeh Riyazi, Frits R. Rosendaal, Rob G. Nelissen, Wayne O. Carter, Marie-Pierre Hellio Le Graverand, and Margreet Kloppenburg. Osteoarthritis of the knee: association between clinical features and MR imaging findings. *Radiology*, 239(3):811–817, June 2006. ISSN 0033-8419. doi: 10.1148/radiol.2393050253.
 - [20] Alex Krizhevsky, Ilya Sutskever, and Geoffrey E Hinton. ImageNet Classification with Deep Convolutional Neural Networks. In *Advances in Neural Information Processing Systems*, volume 25. Curran Associates, Inc., 2012.

- [21] Leon Lenchik, Laura Heacock, Ashley A. Weaver, Robert D. Boutin, Tessa S. Cook, Jason Itri, Christopher G. Filippi, Rao P. Gullapalli, James Lee, Marianna Zagurovskaya, Tara Retson, Kendra Godwin, Joey Nicholson, and Ponnada A. Narayana. Automated Segmentation of Tissues Using CT and MRI: A Systematic Review. *Academic Radiology*, 26(12):1695–1706, December 2019. ISSN 1076-6332. doi: 10.1016/j.acra.2019.07.006. URL <https://www.sciencedirect.com/science/article/pii/S1076633219303538>.
- [22] Geert Litjens, Thijs Kooi, Babak Ehteshami Bejnordi, Arnaud Arindra Adiyoso Setio, Francesco Ciompi, Mohsen Ghafoorian, Jeroen A. W. M. van der Laak, Bram van Ginneken, and Clara I. Sánchez. A survey on deep learning in medical image analysis. *Medical Image Analysis*, 42:60–88, December 2017. ISSN 1361-8415. doi: 10.1016/j.media.2017.07.005. URL <https://www.sciencedirect.com/science/article/pii/S1361841517301135>.
- [23] William Lotter, Greg Sorensen, and David Cox. A Multi-scale CNN and Curriculum Learning Strategy for Mammogram Classification. In M. Jorge Cardoso, Tal Arbel, Gustavo Carneiro, Tanveer Syeda-Mahmood, João Manuel R.S. Tavares, Mehdi Moradi, Andrew Bradley, Hayit Greenspan, João Paulo Papa, Anant Madabhushi, Jacinto C. Nascimento, Jaime S. Cardoso, Vasileios Belagiannis, and Zhi Lu, editors, *Deep Learning in Medical Image Analysis and Multimodal Learning for Clinical Decision Support*, Lecture Notes in Computer Science, pages 169–177, Cham, 2017. Springer International Publishing. ISBN 978-3-319-67558-9. doi: 10.1007/978-3-319-67558-9_20.
- [24] Jun Ma and Bo Wang. Segment Anything in Medical Images, April 2023. URL <http://arxiv.org/abs/2304.12306>. arXiv:2304.12306 [cs, eess].
- [25] Eleftherios A. Makris, Pasha Hadidi, and Kyriacos A. Athanasiou. The knee meniscus: structure-function, pathophysiology, current repair techniques, and prospects for regeneration. *Biomaterials*, 32(30):7411–7431, October 2011. ISSN 0142-9612. doi: 10.1016/j.biomaterials.2011.06.037. URL <https://www.ncbi.nlm.nih.gov/pmc/articles/PMC3161498/>.
- [26] Johanne Martel-Pelletier, Patrice Paiement, and Jean-Pierre Pelletier. Magnetic resonance imaging assessment for knee segmentation and their use in combination with machine/deep learning as predictors of early osteoarthritis diagnosis and prognosis. *Therapeutic Advances in Musculoskeletal Disease*, 15:1759720X231165560, January 2023. ISSN 1759-720X. doi: 10.1177/1759720X231165560. URL <https://doi.org/10.1177/1759720X231165560>. Publisher: SAGE Publications.
- [27] J. Martin Bland and Douglas G. Altman. STATISTICAL METHODS FOR ASSESSING AGREEMENT BETWEEN TWO METHODS OF CLINICAL MEASUREMENT. *The Lancet*, 327(8476):307–310, February 1986. ISSN 0140-6736. doi: 10.1016/S0140-6736(86)90837-8. URL <https://www.sciencedirect.com/science/article/pii/S0140673686908378>.
- [28] Hari McGrath, Peichao Li, Reuben Dorent, Robert Bradford, Shakeel Saeed, Sotirios Bisdas, Sebastien Ourselin, Jonathan Shapey, and Tom Vercauteren. Manual segmentation versus semi-automated segmentation for quantifying vestibular

- lar schwannoma volume on MRI. *International Journal of Computer Assisted Radiology and Surgery*, 15(9):1445–1455, September 2020. ISSN 1861-6429. doi: 10.1007/s11548-020-02222-y. URL <https://doi.org/10.1007/s11548-020-02222-y>.
- [29] Bjoern H. Menze, Andras Jakab, Stefan Bauer, Jayashree Kalpathy-Cramer, Keyvan Farahani, Justin Kirby, Yuliya Burren, Nicole Porz, Johannes Slotboom, Roland Wiest, Levente Lencs, Elizabeth Gerstner, Marc-André Weber, Tal Arbel, Brian B. Avants, Nicholas Ayache, Patricia Buendia, D. Louis Collins, Nicolas Cordier, Jason J. Corso, Antonio Criminisi, Tilak Das, Hervé Delingette, Çağatay Demiralp, Christopher R. Durst, Michel Dojat, Senan Doyle, Joana Festa, Florence Forbes, Ezequiel Geremia, Ben Glocker, Polina Golland, Xiaotao Guo, Andac Hamamci, Khan M. Iftekharrudin, Raj Jena, Nigel M. John, Ender Konukoglu, Danial Lashkari, José Antonio Mariz, Raphael Meier, Sérgio Pereira, Doina Precup, Stephen J. Price, Tammy Riklin Raviv, Syed M. S. Reza, Michael Ryan, Duygu Sarikaya, Lawrence Schwartz, Hoo-Chang Shin, Jamie Shotton, Carlos A. Silva, Nuno Sousa, Nagesh K. Subbanna, Gabor Szekely, Thomas J. Taylor, Owen M. Thomas, Nicholas J. Tustison, Gozde Unal, Flor Vasseur, Max Wintermark, Dong Hye Ye, Liang Zhao, Binsheng Zhao, Darko Zikic, Marcel Prastawa, Mauricio Reyes, and Koen Van Leemput. The Multimodal Brain Tumor Image Segmentation Benchmark (BRATS). *IEEE transactions on medical imaging*, 34(10):1993–2024, October 2015. ISSN 1558-254X. doi: 10.1109/TMI.2014.2377694.
- [30] M Nevitt, D Felson, and Gayle Lester. The osteoarthritis initiative. *Protocol for the cohort study*, 1, 2006. URL <https://nda.nih.gov/static/docs/StudyDesignProtocolAndAppendices.pdf>.
- [31] C. G. Peterfy, E. Schneider, and M. Nevitt. The osteoarthritis initiative: report on the design rationale for the magnetic resonance imaging protocol for the knee. *Osteoarthritis and Cartilage*, 16(12):1433–1441, December 2008. ISSN 1063-4584. doi: 10.1016/j.joca.2008.06.016. URL <https://www.sciencedirect.com/science/article/pii/S1063458408002239>.
- [32] Muhammed Masudur Rahman, Lutz Dürselen, and Andreas Martin Seitz. Automatic segmentation of knee menisci – A systematic review. *Artificial Intelligence in Medicine*, 105:101849, May 2020. ISSN 0933-3657. doi: 10.1016/j.artmed.2020.101849. URL <https://www.sciencedirect.com/science/article/pii/S0933365718307723>.
- [33] Olaf Ronneberger, Philipp Fischer, and Thomas Brox. U-Net: Convolutional Networks for Biomedical Image Segmentation. In Nassir Navab, Joachim Hornegger, William M. Wells, and Alejandro F. Frangi, editors, *Medical Image Computing and Computer-Assisted Intervention – MICCAI 2015*, Lecture Notes in Computer Science, pages 234–241, Cham, 2015. Springer International Publishing. ISBN 978-3-319-24574-4. doi: 10.1007/978-3-319-24574-4_28.
- [34] D. R. Sarvamangala and Raghavendra V. Kulkarni. Convolutional neural networks in medical image understanding: a survey. *Evolutionary Intelligence*, 15(1):1–22, March 2022. ISSN 1864-5917. doi: 10.1007/s12065-020-00540-3. URL <https://doi.org/10.1007/s12065-020-00540-3>.

- [35] Nahian Siddique, Sidike Paheding, Colin P. Elkin, and Vijay Devabhaktuni. U-Net and Its Variants for Medical Image Segmentation: A Review of Theory and Applications. *IEEE Access*, 9:82031–82057, 2021. ISSN 2169-3536. doi: 10.1109/ACCESS.2021.3086020. Conference Name: IEEE Access.
- [36] S. Swain, A. Sarmanova, C. Mallen, C. F. Kuo, C. Coupland, M. Doherty, and W. Zhang. Trends in incidence and prevalence of osteoarthritis in the United Kingdom: findings from the Clinical Practice Research Datalink (CPRD). *Osteoarthritis and Cartilage*, 28(6):792–801, June 2020. ISSN 1063-4584. doi: 10.1016/j.joca.2020.03.004. URL <https://www.sciencedirect.com/science/article/pii/S1063458420309183>.
- [37] Abdel Aziz Taha and Allan Hanbury. Metrics for evaluating 3D medical image segmentation: analysis, selection, and tool. *BMC Medical Imaging*, 15(1):29, August 2015. ISSN 1471-2342. doi: 10.1186/s12880-015-0068-x. URL <https://doi.org/10.1186/s12880-015-0068-x>.
- [38] Lv Tang, Haoke Xiao, and Bo Li. Can SAM Segment Anything? When SAM Meets Camouflaged Object Detection, April 2023. URL <http://arxiv.org/abs/2304.04709>. arXiv:2304.04709 [cs].
- [39] Wolfgang Wirth, Richard B. Frobell, Richard B. Souza, Xiaojuan Li, Bradley T. Wyman, Marie-Pierre Hellio Le Graverand, Thomas M. Link, Sharmila Majumdar, and Felix Eckstein. A three-dimensional quantitative method to measure meniscus shape, position, and signal intensity using MR images: A pilot study and preliminary results in knee osteoarthritis. *Magnetic Resonance in Medicine*, 63(5):1162–1171, 2010. ISSN 1522-2594. doi: 10.1002/mrm.22380. URL <https://onlinelibrary.wiley.com/doi/abs/10.1002/mrm.22380>. _eprint: <https://onlinelibrary.wiley.com/doi/pdf/10.1002/mrm.22380>.
- [40] Junde Wu, Yu Zhang, Rao Fu, Huihui Fang, Yuanpei Liu, Zhaowei Wang, Yanwu Xu, and Yueming Jin. Medical SAM Adapter: Adapting Segment Anything Model for Medical Image Segmentation, May 2023. URL <http://arxiv.org/abs/2304.12620>. arXiv:2304.12620 [cs].
- [41] Hang Yu, Laurence T. Yang, Qingchen Zhang, David Armstrong, and M. Jamal Deen. Convolutional neural networks for medical image analysis: State-of-the-art, comparisons, improvement and perspectives. *Neurocomputing*, 444:92–110, July 2021. ISSN 0925-2312. doi: 10.1016/j.neucom.2020.04.157. URL <https://www.sciencedirect.com/science/article/pii/S0925231221001314>.
- [42] Kaidong Zhang and Dong Liu. Customized Segment Anything Model for Medical Image Segmentation, October 2023. URL <http://arxiv.org/abs/2304.13785>. arXiv:2304.13785 [cs].